Molecular Therapy
Methods & Clinical Development
Original Article

Rescuing the cytolytic function of APDS1 patient T cells via TALEN-mediated PIK3CD gene correction

Lucie Poggi,[1,2] Loïc Chentout,[1,2] Sabrina Lizot,[3] Alex Boyne,[4] Alexandre Juillerat,[4] Arianna Moiani,[3] Marine Luka,[5,6] Francesco Carbone,[5,6] Mickael Ménager,[5,6] Marina Cavazzana,[1,7] Philippe Duchateau,[4] Julien Valton,[3] and Sven Kracker[1,2]

[1]Université de Paris Cité, Imagine Institute, Paris, France; [2]Laboratory of Human Lymphohematopoiesis, INSERM UMR 1163, Paris, France; [3]Cellectis, 8 rue de la Croix Jarry, 75013 Paris, France; [4]Cellectis, Inc., 430 East 29th Street, New York, NY 10016, USA; [5]Université de Paris Cité, Imagine Institute, Laboratory of Inflammatory Responses and Transcriptomic Networks in Diseases, Atip-Avenir Team, INSERM UMR 1163, 75015 Paris, France; [6]Labtech Single-Cell@Imagine, Imagine Institute, INSERM UMR 1163, 75015 Paris, France; [7]Biotherapy Clinical Investigation Center, Groupe Hospitalier Universitaire Ouest, Assistance Publique-Hôpitaux de Paris, INSERM, Paris, France

Gain-of-function mutations in the *PIK3CD* gene result in activated phosphoinositide 3-kinase δ syndrome type 1 (APDS1). This syndrome is a life-threatening combined immunodeficiency and today there are neither optimal nor long-term therapeutic solutions for APDS1 patients. Thus, new alternative treatments are highly needed. The aim of the present study is to explore one therapeutic avenue that consists of the correction of the *PIK3CD* gene through gene editing. Our proof-of-concept shows that TALEN-mediated gene correction of the mutated *PIK3CD* gene in APDS1 T cells results in normalized phospho-AKT levels in basal and activated conditions. Normalization of PI3K signaling was correlated to restored cytotoxic functions of edited CD8+ T cells. At the transcriptomic level, single-cell RNA sequencing revealed corrected signatures of CD8+ effector memory and CD8+ proliferating T cells. This proof-of-concept study paves the way for the future development of a gene therapy candidate to cure activated phosphoinositide 3-kinase δ syndrome type 1.

INTRODUCTION

Activated phosphoinositide 3-kinase δ syndrome (also known as APDS type 1 or APDS1) is a rare but devastating disease resulting in a combined immunodeficiency. Immunological features include decreased serum IgA and IgG levels, increased IgM levels, B cell lymphopenia, increased frequency of transitional B cells, decreased numbers of naive CD4 and naive CD8 cells, and increased numbers of CD8 effector/memory T cells. APDS1 patients show variable clinical manifestations even among the same family.[1–3] Around 98% of patients suffer from recurrent respiratory tract infections indicating an antibody deficiency. Sixty percent have bronchiectasis and chronic viral infections, concomitant to T cell function impairment. Patients can be affected with lymphoproliferation, autoimmune cytopenia, and enteropathy. B lymphoma was also reported in 13% of patients.[3]

APDS1 is caused by gain-of-function (GoF) mutations within the *PIK3CD* gene encoding the class IA PI3K catalytic subunit p110δ, which is predominantly expressed in leukocytes.[4] In normal conditions, activation of the PI3K pathway through several membrane receptors, including T and B cell receptors, cytokine receptors, and co-stimulatory membrane molecules, leads to the phosphorylation of downstream molecules including AKT and ribosomal protein S6. GoF mutations of the *PIK3CD* gene cause a hyperactivation of this signaling pathway. Two independent reports identified heterozygous missense mutations in *PIK3CD*. Among them are the E1021K mutation[2]—which appeared as the most frequent one—and N334K and E525K.[1] Further APDS1-causing gene mutations were then described (E81K, G125D,[5] and R405C,[6] among others). In addition, biallelic loss-of-function (LoF) mutations in *PI3KCD* leading to the decrease, or complete loss of p110δ, have been reported as responsible for a combined immunodeficiency.[7,8] Both LoF and GoF mutation of p110δ results in immune defects, illustrating that a fine balance of PI3Kδ activity is required for proper cell function.

Approved treatments for APDS1 consist in prophylactic measures including long-term antibiotics and Ig replacement therapy.[3] In addition, rapamycin (Sirolimus) treatment targeting mammalian target of rapamycin, a downstream signaling component of the PI3K δ-signaling pathway and a regulator of cell proliferation, was found to successfully decrease lymphoproliferation.[9] Studies using selective PI3Kδ inhibitors, Leniolisib[10,11] and Seletalisib,[12] reported a reduction in lymphadenopathy and normalization of immune B cell

Received 12 May 2023; accepted 5 October 2023; Published: October 23, 2023.
https://doi.org/10.1016/j.omtm.2023.101133.

Correspondence: J. Valton, Cellectis, 8 rue de la Croix Jarry, 75013 Paris, France.
E-mail: julien.valton@cellectis.com
Correspondence: S. Kracker, Université de Paris Cité, Imagine Institute, Paris, France.
E-mail: sven.kracker@inserm.fr

This is an open access article under the CC BY-NC-ND license (http://creativecommons.org/licenses/by-nc-nd/4.0/).

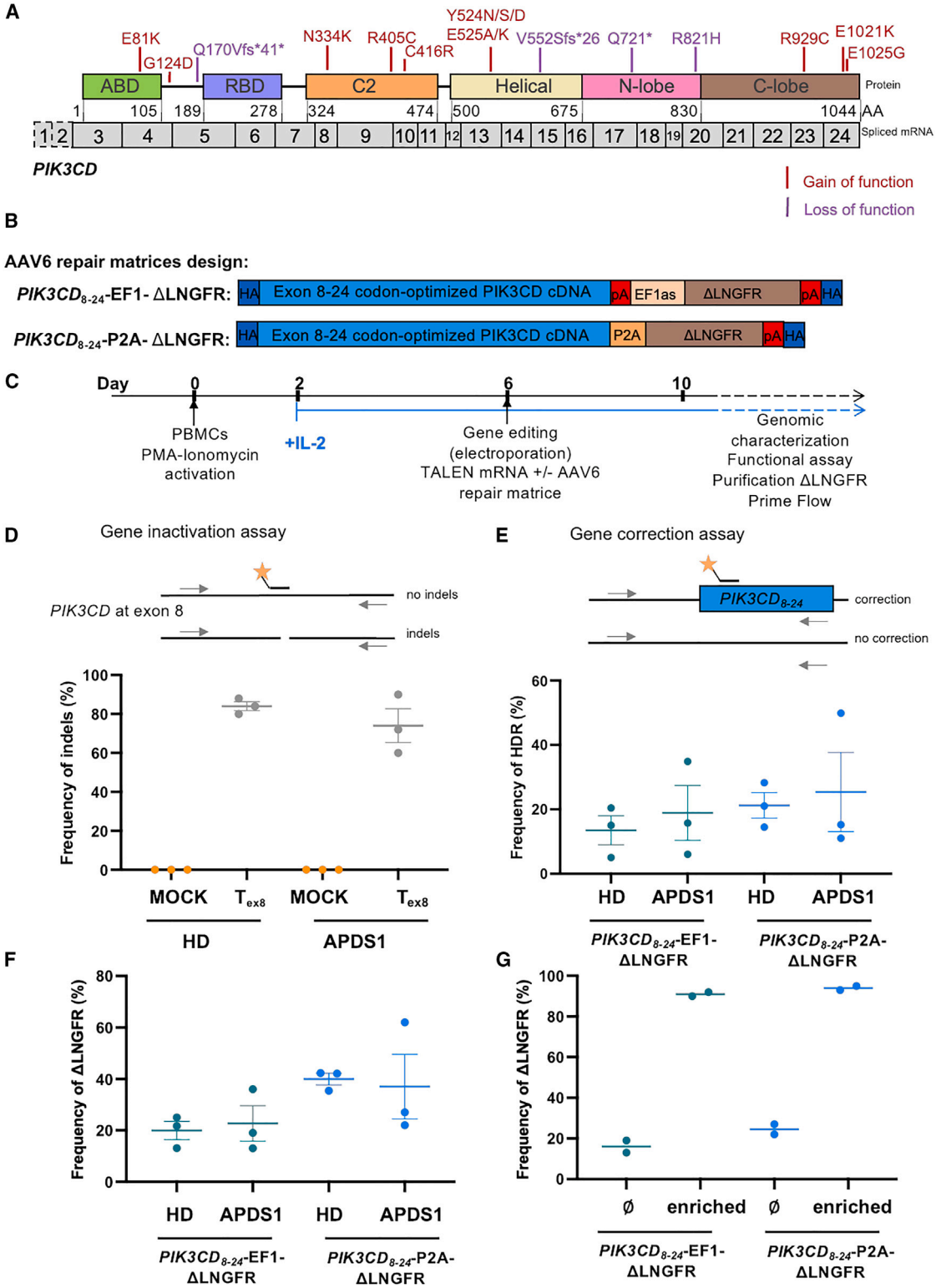

(legend on next page)

subpopulations. Finally allogeneic hematopoietic stem/progenitor cell (HSPC) transplantation has been proposed as a definitive treatment for APDS1. However, the lack of a compatible donor as well as graft failure, graft instability, and poor graft function are still major challenges that must be overcome to reach a positive therapeutic outcome.[13] Thus, so far there are neither optimal nor long-term therapeutic solutions for APDS1 patients and new alternative treatments are highly needed.

The aim of the present study is to explore one of these alternative therapeutic strategies by correcting the mutated *PIK3CD* gene associated to APDS1. We describe a TALEN-mediated gene insertion strategy in which the majority of the mutated *PIK3CD* gene is corrected by its functional sequence in a precise targeted manner. Our results show efficient gene insertion in healthy donor (HD) and APDS1 patient T cells, normalization of PI3K signaling, and rescue of T cell cytotoxic functions. This proof-of-concept study paves the way for the future development of a gene therapy candidate to cure APDS1.

RESULTS

The *PIK3CD* gene can be efficiently edited in HD and APDS1 patient T cells

A large number of GoF mutations, spread across the entire sequence of *PIK3CD* gene, have been associated to APDS1 (Figure 1A).[1,2,5,6,14–20] Similarly, compound heterozygous and/or autosomal recessive LoF mutations have been linked to combined immunodeficiency (Figure 1A).[7,8,21]

Given the large number of mutations associated to APDS1, targeted gene correction of *PIK3CD* appears to be one of the most pragmatic strategies to restore its genetic integrity. Targeted gene correction via homology-directed repair is possible in primary T cells and involve the use of AAV6 or naked DNA repair matrices along with site-specific engineered nucleases including zinc finger nucleases, CRISPR-Cas9, and TALEN.[22,23] To set up an efficient gene correction approach to correct *PIK3CD*, we designed a TALEN named T_{ex8}, targeting the exon 8 coding sequence. This locus was chosen because the correction of the *PIK3CD* gene from exon 8 to 24 would address most LoF and GoF mutations including E1021K, the most prevalent one (Figure 1A). In parallel, two different AAV6 repair matrices were generated to repair *PIK3CD* from exon 8 to 24. The first repair matrix, named $PIK3CD_{8\text{-}24}$-EF1-ΔLNGFR, contained a codon-optimized cDNA encompassing exons 8 to 24 of *PIK3CD* followed by a truncated ΔLNGFR reporter cassette driven by an independent promoter (EF1α) (Figure 1B).[24] The short EF1α promoter sequence was chosen in this case to allow for the packaging of the two large cDNA cassettes (the largest affordable, exons 8 to 24, and LNGFR) in AAV6 particles. The second matrix, named $PIK3CD_{8\text{-}24}$-P2A-ΔLNGFR, followed the same design except that the ΔLNGFR was linked to the cDNA of exons 8 to 24 of *PIK3CD* via a 2A-self-cleaving sequence (P2A). This architecture enables to place ΔLNGFR expression under the control of *PIK3CD* endogenous promoter. Each matrix was flanked by homology arms to enable targeted homology-directed recombination (HDR) at exon 8 of the *PIK3CD* locus. A similar strategy was designed to target exon 17 of *PIK3CD* (with a TALEN named T_{ex17}), another position predicted to be amenable to efficient TALEN gene editing (Figure S1A). Two matrices named $PIK3CD_{17\text{-}24}$-2A-ΔLNGFR and $PIK3CD_{17\text{-}24}$-PGK-ΔLNGFR were designed. Of note regarding the latter matrix, because the cDNA encoding exons 17 to 24 was shorter than its exon 8 to 24 counterparts, we could afford to replace the short EF1α with the larger PGK promoter, known to elicit higher transgene expression (LNGFR in this case).

T cells from HD and APDS1 patients carrying the E1021K mutation were enriched via **peripheral blood mononuclear cell** (PBMC) activation by PMA/ionomycin, a nonspecific agent inducing signaling in T cells (Figure 1C).[25,26] This activation method was favored over the conventional anti-CD3/CD28 bead activation to preserve the already-elevated PI3K intracellular signaling of APDS1 T cells and avoid activation-induced cell death (AICD).[2] Following activation, T cells were propagated in the presence of interleukin-2 (IL-2) and edited 6 days after activation with T_{ex8} or T_{ex17}, in the presence or absence of their corresponding AAV6 repair matrices.

Quantification of gene editing events promoted by TALEN treatment in the absence of any AAV6 repair matrix showed that T_{ex8} treatment elicited high levels of insertion and deletion events (indels) in both HD and APDS1 T cells (80% and 74%, respectively, Figure 1D). These digital-droplet PCR (ddPCR)-based quantifications of indel frequency were confirmed by next-generation sequencing (Figure S1B). Similar results were obtained with T_{ex17}, albeit with lower frequencies of indels (Figure S1C, left panel). In addition, the integration of the matrices targeting exon 8, measured at the genomic level by ddPCR, showed up to 20% and 30% integration rate of $PIK3CD_{8\text{-}24}$-EF1-ΔLNGFR and $PIK3CD_{8\text{-}24}$-P2A-ΔLNGFR, respectively, in both HD and APDS1 cells (Figure 1E). Similar integration rates were determined by flow cytometry based on ΔLNGFR expression confirming our genomic results (Figure 1F). The integration of the AAV6 matrices targeting exon 17 resulted in similar integration rates, ranging from 10% to 30% (Figure S1C, right panel).

Figure 1. *PIK3CD* gene correction in healthy donor and APDS1 patient T cells using TALEN and AAV targeting exon 8 of *PIK3CD*

(A) Schematic of the p110δ protein. Loss-of-function and gain-of-function mutations associated to human immunodeficiencies are indicated. Corresponding mRNA coding region is indicated underneath. Exons 1 and 2 are not coding. *, stop codon; fs, frameshift. (B) Schematic of the AAV-encoded repair matrices for exon 8 targeting. pA, poly(A); EF1as, EF1 alpha short promoter; trLNGFR, truncated LNGFR. (C) Timeline of gene editing procedure. (D) Design of ddPCR assay to assess indels at the targeted locus after induction of T_{ex8} or T_{ex17}. Frequency of unmodified allele: (NHEJ – unmodified conc./RPP30 conc.) × 100. (E) Design of ddPCR assay to assess HDR at exon 8. Frequency of HDR allele: (HDR conc./RPP30 conc.) × 100. (F) Flow cytometry analysis of LNGFR expression by healthy donor (HD) cells and APDS1 cells modified with both repair matrices targeting exon 8. (G) Flow cytometry analysis of LNGFR-positive cells obtained before and after enrichment with magnetic beads on two different patients. ∅, not enriched condition. Error bars represent the mean of Indels, HDR and ΔLNGFR frequencies +/- standard error of mean (SEM).

We then aimed to purify ΔLNGFR(+) T cells by magnetic selection. In the context of this proof-of-concept study, this step enables to enrich for T cells containing mono- and biallelic gene corrective events and thus allows for a more rigorous downstream functional characterization of the outcome of gene correction. Our results showed that ΔLNGFR surface expression allowed for efficient magnetic enrichment of gene edited APDS1 T cells with up to 90% of purity obtained with both repair matrices targeting exon 8 (Figure 1G).

Correlation between ΔLNGFR, endogenous *PIK3CD* (*PIK3CD* WT) and $PIK3CD_{8\text{-}24}$ mRNA expression is important to ensure that the enriched cells were effectively modified at the intended locus. Prime flow RNA assay was used to analyze the levels of *PIK3CD* WT and $PIK3CD_{8\text{-}24}$ transcripts at the single-cell level as well as the expression of the ΔLNGFR surface marker in APDS1 patient T cells (Figure 2A). Interestingly, our results showed that the endogenous level of *PIK3CD* WT mRNA was not affected by T_{ex8} treatment in the absence of AAV6 repair matrix (Figure 2B). This suggested that T_{ex8} editing did not trigger non-sense mediated decay of *PIK3CD* mRNA. However, by design, *PIK3CD* mRNA level was reduced in the presence of the repair matrices, and was correlated to an increase of $PIK3CD_{8\text{-}24}$ transcripts, especially in edited cells (Figure 2C, compare *PIK3CD* WT and $PIK3CD_{8\text{-}24}$ MFI obtained in ΔLNGFR(+) T cells and in ΔLNGFR(−) cells). This indicated a correlation between *PIK3CD* gene correction and $PIK3CD_{8\text{-}24}$ insertion and confirm that ΔLNGFR expression correlates with $PIK3CD_{8\text{-}24}$ expression (Figure 2C). These observations were reproducible across two different APDS1 patient T cell and HD T cell batches. Together, these data showed that *PIK3CD* gene correction successfully occurred in HD and APDS1 patient T cells treated by T_{ex8} and each of the AAV6 repair matrices (either $PIK3CD_{8\text{-}24}$-EF1-ΔLNGFR or $PIK3CD_{8\text{-}24}$-P2A-ΔLNGFR).

Overall, our data showed that the *PIK3CD* gene can be efficiently modified in HD and APDS1 T cells through a gene editing process involving TALEN and AAV6 repair matrix treatment and that modified cells can be efficiently enriched using the ΔLNGFR surface marker.

TALEN-mediated *PIK3CD* gene correction normalizes PI3K signaling in APDS1 patient T cells

Elevated AKT phosphorylation levels in both basal and activated conditions is a well-established hallmark of APDS1.[5,27,28,29] Hence, phospho-AKT (pAKT) levels in APDS1 and APDS1-corrected T cells were investigated and compared to evaluate the functional outcome of our gene correction strategy. As a reference, HD T cells, either untreated or treated with the same gene correction process, were used to determine normal pAKT levels and to test the functionality of the repair matrices. Our results showed that APDS1 T cells exhibited a higher level of phosphorylation compared with HD T cells, before (basal level) and after being activated by a CD3-specific antibody activator named OKT3 (Figures 3A, 3B, and S2A). Treatment with a p110δ-specific inhibitor abrogated those differences, confirming that PI3Kδ signaling was responsible for the high level of AKT phosphorylation observed in both conditions (Figures S2A and S2B). Interestingly, APDS1 T cells treated with T_{ex8} alone showed a reduction in basal and activated pAKT levels, indicative of a p110δ inactivation. In contrast, ΔLNGFR(+) APDS1 T cells edited by T_{ex8} in the presence of one of the two repair matrices showed full normalization of pAKT basal levels, while still being activated by OKT3, up to the normal levels obtained in HD. These results were reproduced in HD T cells. Indeed, HD cells and ΔLNGFR(+) corrected HD cells showed similar levels of activation while T_{ex8}-treated HD T cells showed a reduced pAKT level after OKT3 activation (Figure S2A). Finally, similar results were observed with APDS1 and HD T cells edited at exon 17 (Figures 3B and S2B). CD4/CD8 ratios of cultured cells were also measured while measuring pAKT (Figures S3A and S3B).

Together, these data indicate that the TALEN-mediated *PIK3CD* gene correction strategy (at both exons 8 and 17) normalized pAKT basal and activated levels of APDS1 T cells to that obtained in HD T cells. The next sections focuses on the characterization of HD and APDS1 T cells engineered at exon 8 because this approach enables to correct a higher amount of mutations compared with its counterpart performed at exon 17.

TALEN-mediated *PIK3CD* gene correction rescues the cytolytic activity of APDS1 patient CD8+ T cells

Since our *PIK3CD* gene correction process elicited a normalization of pAKT levels of APDS1 T cells, we logically sought to further investigate its effect on the cytolytic activity of corrected APDS1 T cells using a sensitive serial killing assay. For that purpose, we used blinatumomab,[30] a bispecific T cell engager antibody crosslinking CD3 and CD19, to mediate T cell-dependent killing of luciferase-mCherry-expressing B-EBV cells (Figure 4A). HD and APDS1 T cells were engineered according to the protocol described earlier and expanded using one round of activation to get a homogeneous population of CD8+ T cells, the subpopulation of choice to assess the cytolytic activity of T cells (Figure S4A). Expanded CD8+ T cells, were challenged by daily addition of B-EBV cells for 1 week and their proliferation and cytotoxic activity was assessed by flow cytometry and B-EBV luminescence signaling, respectively (Figure 4B).

Regarding the proliferation of T cell in the presence of B-EBV, our flow cytometry results showed that uncorrected and corrected HD T cells displayed a similar drop of T cell count over time (Figure 4C). This pattern was expected because of the lack of T cell proliferation signal or proliferation-prone cytokines in this assay. Interestingly, this drop of T cell count was significantly more pronounced for APDS1 than for HD uncorrected T cells (Figures 4C and 4D, compare counts obtained at day 7 in HD and APDS1 uncorrected T cells, $p = 0.0149$), a phenomenon consistent with the reported increased AICD in APDS1 T cells.[2] In contrast, the enriched $PIK3CD_{8\text{-}24}$-EF1-ΔLNGFR APDS1 CD3+ T cell count obtained at day 7 was significantly higher than the one obtained for uncorrected APDS1 cells

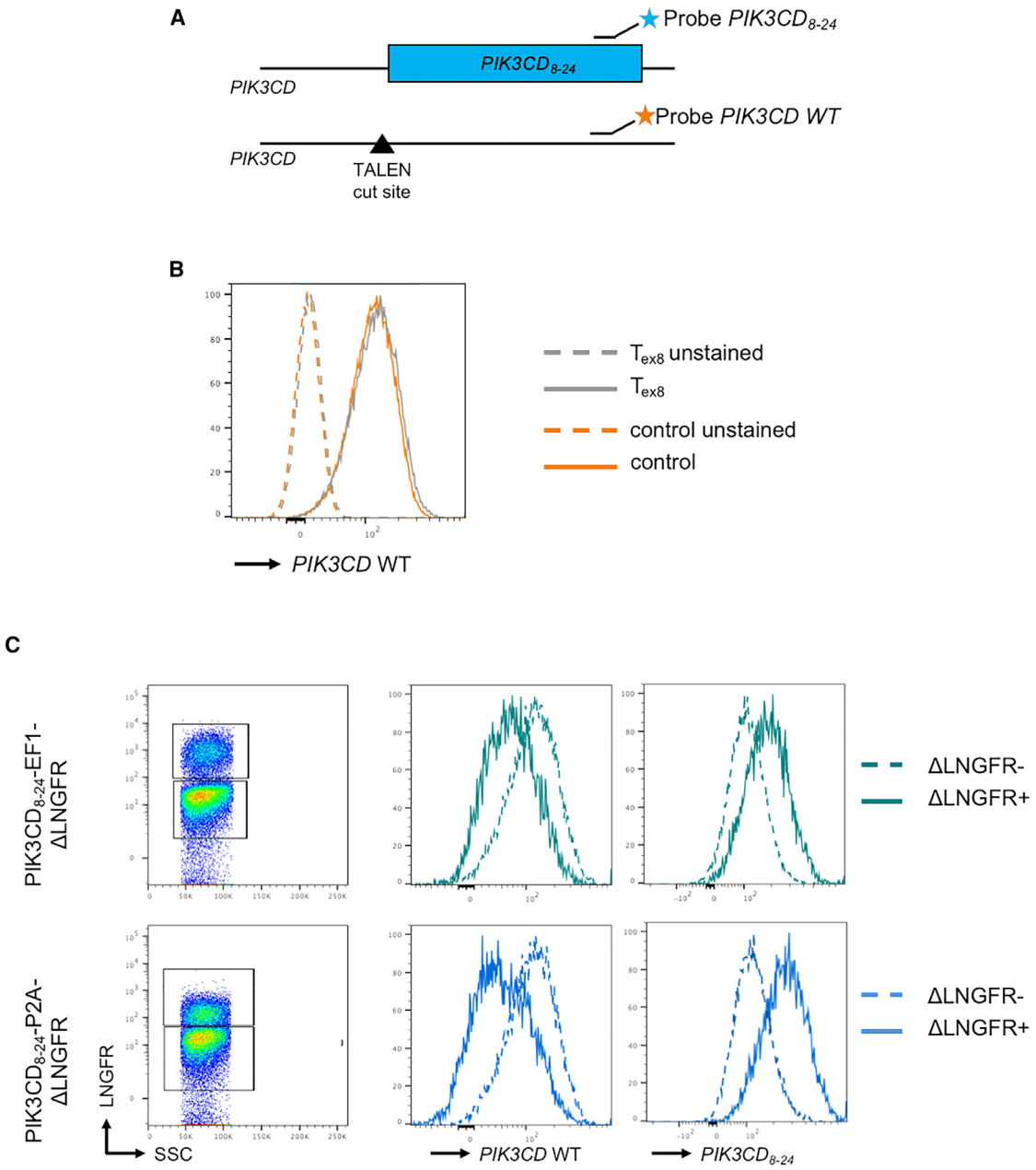

Figure 2. Prime flow analysis of APDS1 patient T cells treated with TALEN in the presence or absence of AAV targeting exon 8 of *PIK3CD*

(A) Schematic of the probe design for prime flow RNA assay at the *PIK3CD* locus. (B) Histogram overlay of control and T_{ex8}-treated T cells illustrating the expression of endogenous *PIK3CD* WT. The dashed line indicates unstained control. (C) Left column: FACS plot LNGFR/SSC and gating on LNGFR-positive and -negative cells. (C) Middle column: histogram overlay of the expression of endogenous *PIK3CD* WT in corrected cells. (C) Right column: histogram overlay of the expression of $PIK3CD_{8-24}$ in corrected cells. Histograms illustrate representative result obtained on two independent experiments performed with HD and APDS1 T cells. The dashed line indicates unstained LNGFR-negative cells and the solid line indicates LNGFR-positive cells.

(Figure 4D, p = 0.0103), and similar to the ones obtained for uncorrected and corrected HD T cells (Figure 4C, non-significant p = 0.8190 and p = 0.4547, respectively). This pattern suggested that the gene correction process improved the fitness of the corrected APDS1 T cells and potentially, their ability to cope with AICD.

Regarding cytolytic activity of T cells, we found that both uncorrected and corrected HD T cells were able to efficiently control B-EBV growth. This was demonstrated by the evolution of B-EBV levels throughout the assay, that were found significantly lower in the presence than in the absence of corrected or uncorrected HD T cells

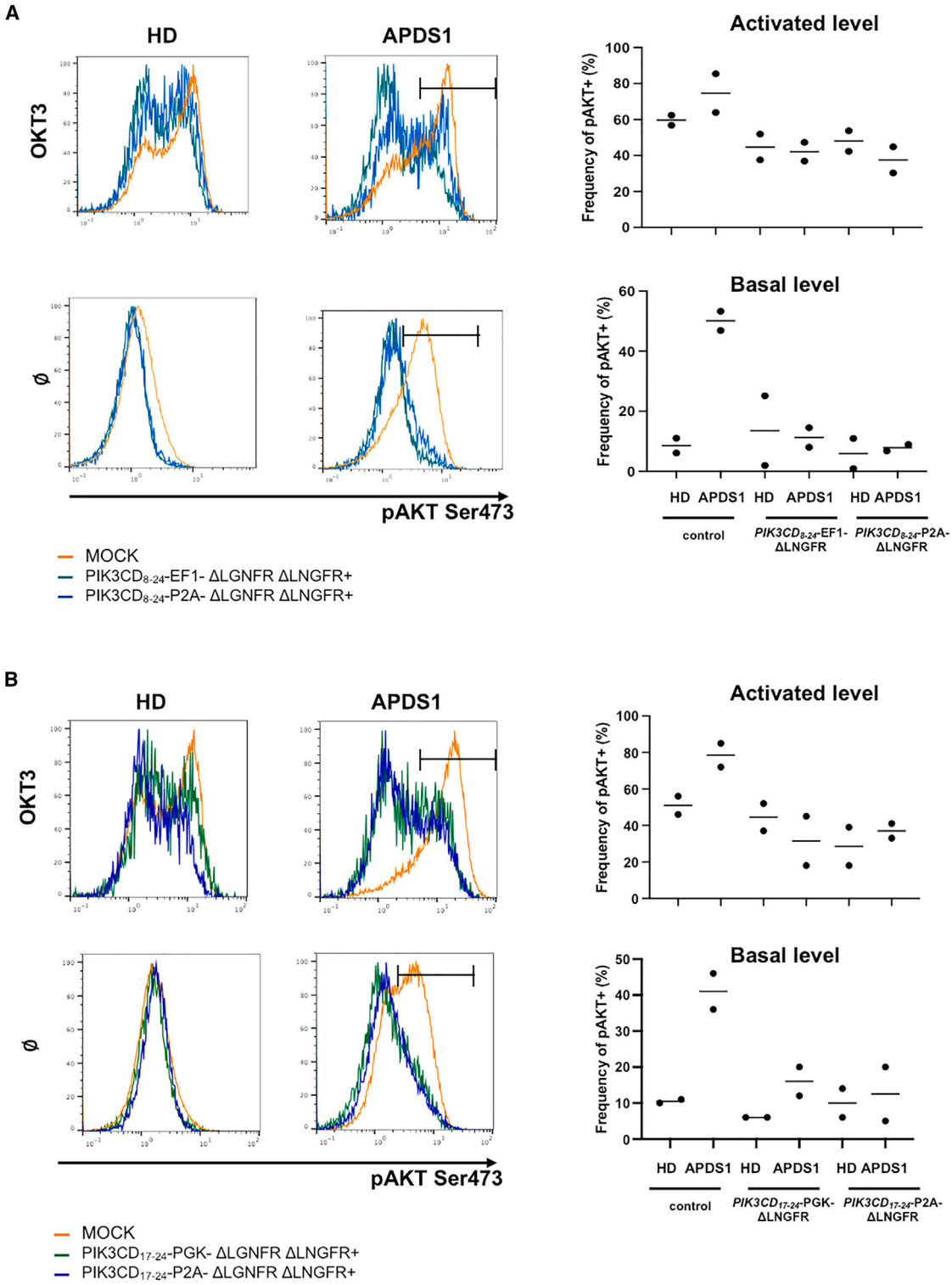

Figure 3. *PIK3CD* gene correction normalizes phospho-AKT levels in APDS1 T cells

(A) Left panels: histograms showing phospho-AKT levels (pAKT Ser473) obtained in the presence or absence of OKT3 in HD and APDS1 patient T cells modified at exon 8 with both exon 8-specific matrices. Signals obtained with unmodified and ΔLNGFR (+) edited T cells are displayed. Gating strategy enabling the quantification of basal and activated levels of phosphor-AKT is displayed as a horizontal bar. Right panel: quantification of basal and activated levels of phosphor-AKT detected in HD and APDS1 patient

(legend continued on next page)

(Figure 4E, $p < 0.0001$). In stark contrast, uncorrected APDS1 T cells failed to control B-EBV growth, as shown by the similar levels of B-EBV obtained in the presence and absence of T cells at day 7 (Figure 4F). Interestingly, this lack of B-EBV control was efficiently rescued by the gene correction process. Indeed, we found that the cytolytic activity of enriched *PIK3CD*$_{8\text{-}24}$-EF1-ΔLNGFR APDS1 T cells was significantly higher than uncorrected APDS1 T cells and equivalent to uncorrected and corrected HD T cells throughout the assay (Figures 4E and 4F, $p = 0.0013$, $p = 0.6308$, and $p = 0.7495$, respectively). A similar trend was observed for APDS1 T cell corrected by the *PIK3CD*$_{8\text{-}24}$-P2A-ΔLNGFR matrix, further confirming of our results, and demonstrating that both correction strategies led to an efficient rescue of the cytolytic function of APDS1 T cells (Figure S4B).

Transcriptomic characterization of *PIK3CD* corrected APDS1 patient cells

We found that TALEN-mediated *PIK3CD* gene correction of APDS1 T cells efficiently normalized the cytolytic activity of the CD8+ T cell subpopulation. To further understand and characterize the basis of such normalization, we performed an in-depth single-cell transcriptomic comparative analysis between HD T cells and APDS1 T cells, the latter being either uncorrected or corrected by the T_{ex8} and *PIK3CD*$_{8\text{-}24}$-EF1-ΔLGNFR matrix treatment. We reasoned that comparing untreated with corrected APDS1 T cells would enable characterization of the effect of the gene editing procedure and better understand its downstream biological consequences while comparing untreated HD with APDS1 T cells would unravel PI3Kδ-related signaling defects associated to APDS1.

For that purpose, HD and APDS1 PBMCs were thawed, activated, and edited using the protocols described earlier, before being further expanded. The length of the cell culture was extended to remove any ectopic expression of the non-integrated *PIK3CD*$_{8\text{-}24}$-EF1-ΔLGNFR matrix and to expand the cells up to a number allowing the magnetic enrichment process. Corrected APDS1 cells were enriched based on ΔLNGFR expression 3 days before performing the single-cell RNA sequencing (scRNA-seq) procedure (Figure 5A). This enrichment step (similar outcome as in Figure 1G) was performed to improve the homogeneity of the gene-corrected APDS1 cell pool and prevent the presence of by-standard uncorrected APDS1 cells that would complexify the transcriptomic comparative analysis.

We first sought to identify the different cellular subsets present in the three experimental groups. For that purpose, sequencing data were mapped on a previously published multimodal reference atlas of 162,000 PBMCs (Figure 5B).[31] To validate the different cellular clusters, standard markers were plotted for each of them (Figure S5A). Similar clusters were detected in HD, APDS1, and corrected APDS1 cells (Figure 5B). Of note, we could not find a B cell related cluster selected out by our T cell-selective activation process and cell culture conditions. When focusing on the CD8+ cluster, the cellular population used in our serial killing assay (Figures 4E, 4F, and S5B), we identified four main subpopulations, two of which were found enriched in purified corrected cells, namely CD8 T effector memory (CD8 TEM) and CD8 proliferating cells.

We then investigated and mapped the expression of the *PIK3CD* and *PIK3CD*$_{8\text{-}24}$ transgenes in the different clusters identified. The expression of *PIK3CD*$_{8\text{-}24}$-EF1-ΔLNGFR cassette expression could be theoretically assessed by quantifying the *PIK3CD*$_{8\text{-}24}$ or ΔLNGFR mRNA expression (Figure 5C, top). Due to its higher expression/detection compared with ΔLNGFR, *PIK3CD*$_{8\text{-}24}$ was preferentially used to identify the corrected cells. The *PIK3CD*$_{8\text{-}24}$ cassette expression was detected in all the clusters of the corrected APDS1 cells while not detected in HD and uncorrected APDS1 cells (Figure 5B, middle). In addition, endogenous *PIK3CD* expression was detected in all clusters of HD and APDS1 cells, albeit expressed to a lower level in APDS1 corrected cells, in agreement with the prime flow dataset described earlier (Figures 5B, bottom and 2C). Of note, expression of the endogenous *PIK3CD* was found lower than *PIK3CD*$_{8\text{-}24}$, suggesting a difference of stability and turn over kinetics between the two transcripts. These data indicated that all T cell subsets were amenable to gene editing and that two main clusters, namely CD8 TEM and CD8 proliferating, were enriched by the gene editing and cell culture procedure.

Impact of TALEN-mediated *PIK3CD* gene correction on the transcriptomic status of APDS1 patient CD8+ T cells

Next, we investigated whether the normalization of the cytolytic activity and PI3K signaling found earlier in corrected APDS1 CD8+ T cells were concomitant to global changes in their cellular transcriptome. To do so, we further characterized the transcriptome of corrected APDS1 CD8+ T cells, especially in the two most abundant subsets (CD8 TEM and CD8 proliferating) and compared it with the ones obtained in the same subsets identified in uncorrected APDS1 and HD cells.

Focusing on the CD8 TEM subset, we identified 90 differentially expressed genes (DEGs) between uncorrected and corrected APDS1 T cells (Figure 5C, left panel). To enrich for dysregulated genes linked to APDS1, 70 DEGs between HD and APDS1 cells were identified and intersected to the previous list. From this intersection, 26 common genes were identified, and their average expression was plotted as a heatmap (Figure 5D). This heatmap enabled us to clearly spot genes that were dysregulated by APDS1 and gauge the extent of their normalization after *PIK3CD* gene correction. Among the dysregulated gene population, we identified multiple genes implicated in T cell cytotoxicity (*GNLY*, *GZMH*, *GZMB*, and *GZMK*), in T cell

T cells either unmodified or modified at exon 8 with both exon 8-specific matrices. (B) Left panels: histograms showing phospho-AKT levels obtained in the presence or absence of OKT3 in HD and APDS1 patient T cells modified at exon 17 with both exon 17-specific matrices. Signals obtained with unmodified and ΔLNGFR (+) edited T cells are displayed. Gating strategy enabling the quantification of basal and activated levels of phosphor-AKT is displayed as a horizontal bar. Right panel: quantification of basal and activated levels of phosphor-AKT detected in HD and APDS1 patient T cells either unmodified or modified at exon 17 with both exon 17-specific matrices.

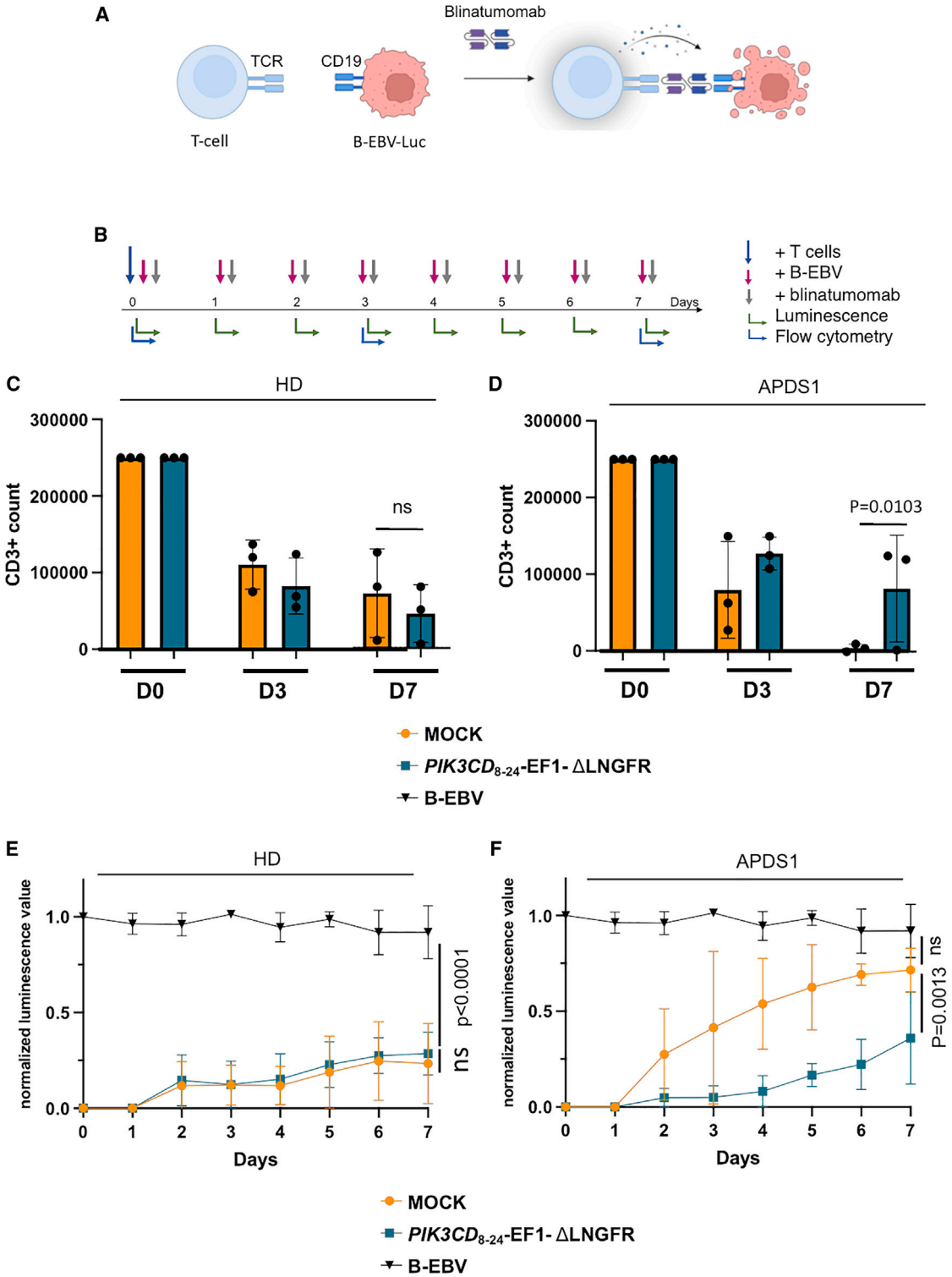

Figure 4. *PIK3CD* gene correction rescues the cytolytic activity in APDS1 T cells

(A) Schematic of blinatumomab-dependent serial killing assay. (B) Schematic of the serial killing assay used to characterize the long-term cytolytic activity of uncorrected and *PIK3CD*$_{8\text{-}24}$-EF1-LGNFR corrected T cells. The sequential addition of T cells, target cells (B-EBV), and blinatumomab, as well as the different flow

(legend continued on next page)

activation, and in antigen presentation (*XCL2*, *CD74*, and *HLA* class II gene family, respectively), and in the PI3K/AKT signaling cascade (*CXCR4* and *KLF2*). Interestingly, their expression level was found to be normalized to the one obtained for HD cells after the *PIK3CD* gene correction process. A similar analysis was carried out on CD8 proliferating cells, focusing on cells in the G2M phase to homogenize the population. Twenty-seven common genes were identified (Figure 5C, middle panel) and again, their transcriptomic signature was found normalized to HD levels (Figure 5D, middle panel).

Among the normalized gene population obtained in CD8 TEM and the G2M CD8 proliferating, 14 were found to be common (Figure 5C, right panel). When subjected to a gene ontology analysis, these common genes were found to be involved in immune response processes, antigen presentation, and T cell activation (Figure 5E). Of note, similar analyses were carried out on other subpopulations that are not commonly associated to the pathophysiological consequences of APDS1 (Figure S6). Although we could observe few individual genes normalized in these subpopulations, we could not demonstrate the normalization of the full list of genes described above. This indicated that the conclusion drawn out of this transcriptomic study are specific to CD8 TEM and CD8 proliferating subsets.

Altogether, our results showed that the mutated *PIK3CD* gene associated to APDS1 can be efficiently corrected by TALEN and AAV6-mediated gene insertion. Mutated *PIK3CD* gene correction resulted in a normalization of pAKT levels and cytolytic activity of APDS1-corrected T cells. This phenomenon could be explained, in part, by the normalization of the transcriptomic signature of genes involved in CD8+ T cell cytolytic activity, although additional work is needed to further specify this point.

DISCUSSION

The aim of this study was to establish a proof-of-concept of a *PIK3CD* gene correction strategy in APDS1 patient cells. Using a TALEN-mediated *PIK3CD* editing along with an AAV6-based DNA repair matrix delivery, we show that the mutated *PIK3CD* allele can be efficiently edited and corrected in APDS1 patient T cells. Corrected T cells display (1) normalized pAKT level, (2) rescue of functional cytotolytic activity, and (3) normalized transcriptomic signature of certain genes involved in CD8+ T cell cytolytic function, activation, and fitness. This work paves the way for the development of a gene therapy approach to treat p110δ dysregulations in a long-term fashion.

Autologous corrected HSPC transplantation represents the ultimate goal for long-lasting curative treatment of APDS1. However, we chose to establish this first proof-of-concept of *PIK3CD* gene correction in APDS1 T cells for multiple reasons. First and foremost, the T cell subsets play a key role in the pathophysiological consequences of the APDS1. Their dysfunctional phenotype, fitness, and cytolytic activity are well characterized, making them a relevant and resourceful cellular model to assess the benefits of *PIK3CD* gene correction. Second, APDS1 T cells could be accessible from APDS1 patient blood donation, thus avoiding the need and burden of complex and potentially dangerous clinical interventions to source our starting materials. Third, thanks to the thorough genomic screening of APDS1 patients, we could selectively choose PBMC specimens harboring the monoallelic E1021K GoF mutation found in 90% of the patients diagnosed to date. The E1021K GoF mutation being the common denominator between the selected donors, we were able to assess the influence of the donor-to-donor variability on the efficiency of our gene correction process and its phenotypic consequences. Finally, establishing this first proof-of-concept in terminally differentiated T cells could inform some of the functional benefits of generating a gene therapy product based on APDS1 HSC editing.

Because of its central role in different cellular functions, the enzymatic activity of p110δ must be tightly regulated at a protein and transcriptomic level. We thus accounted for this feature and designed our gene correction strategy to place the corrective cDNA sequence under the control of the endogenous regulatory elements of *PIK3CD*. To address most LoF mutations (which are biallelic) associated to combined immunodeficiency, and GoF mutations associated to APDS1, we chose two distinct loci (exons 8 and 17) as landing pads for *PIK3CD* repair matrix insertion. Both loci were efficiently edited by their respective TALEN with frequencies of indels ranging from 30% to 85%. This level of indels was correlated to a partial decrease of p-AKT level upon OKT3 activation, indicating p110δ inactivation (Figure S2). Surprisingly, we did not find any clear evidence for non-sense-mediated decay of *PIK3CD* edited transcripts, a phenomenon seen in different instances after gene editing.[32]

TALEN-mediated editing in the presence of *PIK3CD* repair matrix elicited up to 50% of *PIK3CD* correction in APDS1 T cells. This efficiency was affected by the size of the *PIK3CD* repair matrices, a size dictated by the exon targeted and, as a corollary, by the length of CDNA needed to correct the *PIK3CD* gene. In agreement with previous works,[33] for a given locus edited by a given TALEN, the higher the size of the lower integration rate, as exemplified by the difference of gene insertion obtained with $TALEN_{ex8}$ at exon 8 with $PIK3CD_{8\text{-}24}$-P2A-ΔLNGFR (3.8 kb) compared with $PIK3CD_{8\text{-}24}$-EF1-ΔLNGFR (4.3 kb) and with

cytometry and luminescence measurements performed throughout the assay are indicated. (C and D) CD3+ cell counts obtained over time for three HD and three patient donors. (E and F) Normalized luciferase measurement obtained over time with B-EBV alone or B-EBV mixed with the experimental groups described above. The normalized luminescence value was calculated as the ratio of luminescence obtained in the presence over the one obtained in the absence of blinatumomab. The error bars illustrated in C and D represent the mean of CD3+ counts obtained with 3 independent donors +/- standard deviation (SD) and statistical analysis were performed using a on one-way ANOVA test. The error bars illustrated in E and F represent the mean of normalized luminescence obtained with 3 independent donors +/- standard deviation (SD). Statistical analysis were performed using a student's t-test and the area under the curve as metrics. *p*-value are indicated. Significance was defined as p-value < 0.05. ns = not significant.

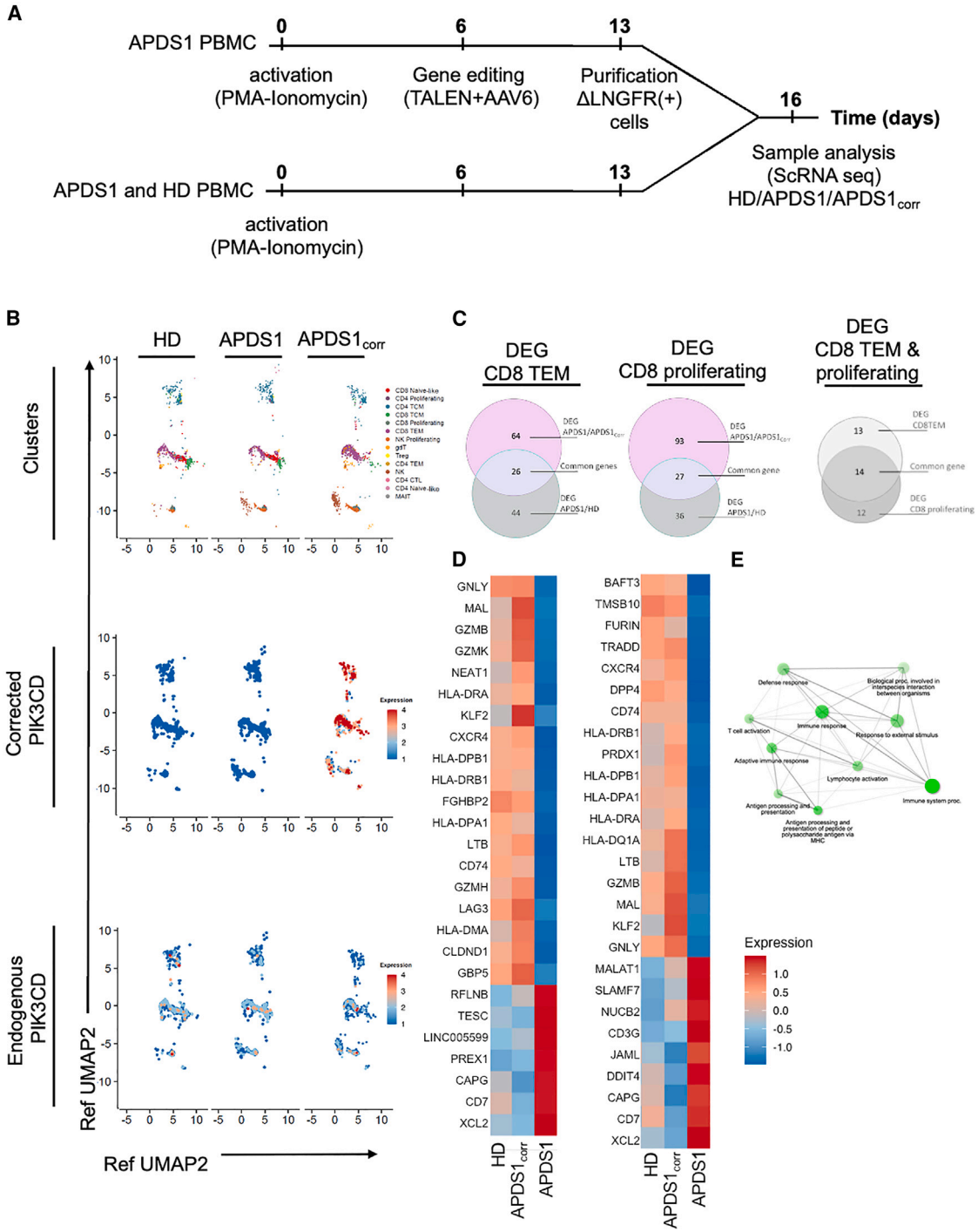

Figure 5. Deciphering the outcome of *PIK3CD* gene correction via by single-cell transcriptomics

(A) Timeline of the gene editing process and time point of sample analysis. (B) UMAP of HD, APDS1, and corrected APDS1 T cells (APDS1corr). Top: identified clusters. Middle: expression of the $PIK3CD_{8\text{-}24}$ cassette. Bottom: expression of endogenous *PIK3CD*. (C) Venn diagram of DEGs in the clusters CD8 TEM (left) and CD8 proliferating (middle). Right panel: Venn diagram of corrected genes found in both clusters CD8 TEM and CD8 proliferating. (D) Heatmap of the common genes in the CD8 TEM cluster (left) and the CD8 proliferating cluster (right). (E) Gene ontology analysis of all the corrected DEGs. Proc., processes.

$TALEN_{ex17}$ at exon 17 with *PIK3CD*$_{17\text{-}24}$-P2A-ΔLNGFR (3.1 kb) compared with *PIK3CD*$_{17\text{-}24}$-PGK-ΔLNGFR (3.8 kb).

Insertion of the *PIK3CD*$_{8\text{-}24}$ repair matrices elicited an efficient transcription of their corresponding mRNA. Surprisingly, while being under the control of *PIK3CD* endogenous promoter, *PIK3CD*$_{8\text{-}24}$ transcripts displayed a higher stability compared with their endogenous counterparts (Figure 5B). This could be due to their distinct 3′ untranslated region. Indeed, this region is known to play a role in the downregulation of *PIK3CD* expression through the action of MicroRNA-7.[34] Other factors including the codon optimization of the *PIK3CD*$_{8\text{-}24}$ cassette and its synthetic poly(A) sequence may also account for the improved stability of the corrective transcript.

In most of the cases, APDS1 patients are heterozygous carriers of dominant GoF mutations. Thus, our gene correction strategy must target the mutated dysfunctional allele to be effective. The strategy we have chosen is not specific to the mutated allele responsible for APDS1. Hence, depending on the efficiency of gene correction, edited cells could harbor different genotypes ranging from unedited to mono- and biallelic *PIK3CD* gene correction or inactivation including mixed genotypes. While the ΔLNGFR purification allows setting aside cells harboring no editing or mono-/biallelic *PIK3CD* inactivation, it cannot do so with cells carrying a functional corrected allele and a dysfunctional mutated allele. These remaining cells could thus theoretically dampen the therapeutic benefit of the gene correction process because of the dominant nature of the APDS1 E1021K mutation. However, our functional assays argue against that. Indeed, although an additional genotypic characterization of edited cells may be informative, the rescue of phosphor-AKT levels and CD8+ T cell cytolytic activity observed in our functional assays suggest that the frequency of corrected cells carrying one dysfunctional allele is low enough for this treatment to be beneficial. In addition, because of the high activity of the TALEN (indels ∼80%), it is very likely that purified cells bearing only one corrected allele also bear one inactivated allele. This feature could decrease the probability of generating corrected cells carrying one mutated dysfunctional allele, an important benefit for the treatment of GoF mutations associated to APDS1. Further work would be needed to thoroughly address this point.

Nevertheless, one way to increase the number of cells harboring therapeutically relevant gene correction events would be to selectively purify cells containing biallelic *PIK3CD* correction. This could be achieved by performing a double transduction of APDS1 T cells with two AAV6 corrective matrices carrying distinct cell surface markers including, for instance, an LNGFR and a truncated EGFR.[35] Purification of cells expressing both surface markers would theoretically lead to a homogeneous population of biallelically corrected cells. Although testing this approach is outside the scope of this study, it could enable to selectively purify therapeutically relevant cells carrying biallelic *PIK3CD* gene correction.

Normalization of the cytolytic activity of corrected APDS1 patient CD8+ T cells was associated with a recovery of conventional expression profile of genes involved in T cell cytotoxicity, T cell activation, and T cell fitness, especially in CD8 TEM and CD8 proliferating subsets. These results suggest that correction of *PIK3CD* leads to a reset of ADPS1 CD8+ T cell transcriptomics status. This transcriptomics reset was, however, not global. Indeed, we did not find full overlap of DEGs found between the uncorrected/corrected APDS1 group and HD/APDS1 group (Figure 5C). This partial normalization could be due to donor-to-donor variability between the HD and APDS1 patient T cells, a variability that may be influenced by their distinct epigenetic status as well as differentiation processes. We hypothesize that while our gene correction strategy could repair the function of terminally differentiated CD8+ APDS1 T cells, it may not be able to rewrite their biological history shaped during differentiation. One way to investigate this assumption and increase the power of our analysis would be to reproduce these results on multiple HD and APDS1 donors, using edited and non-edited HSPCs and their corresponding T cells, differentiated *in vitro* in a controlled manner.

The positive outcome of *PIK3CD* gene correction on APDS1 T cell functions reported in this study warrants further development of a long-term curative treatment for APDS1 patients. To that matter, the correction of *PIK3CD* gene in HSPCs mobilized from APDS1 patients may represent a valid option to develop such a treatment. By design, the *PIK3CD* repair matrices targeting exons 8 and 17 (*PIK3CD*$_{8\text{-}24}$-EF1-ΔLNGFR and *PIK3CD*$_{17\text{-}24}$-PGK-ΔLNGFR) could be transposable to HSPC editing and purification. Indeed, they both incorporate a constitutively expressed reporter gene that would allow for efficient purification of HSPC-corrected cells before their differentiation. In addition, this approach could be highly informative from a mechanistic standpoint. Indeed, it could allow characterizing the influence of *PIK3CD* gene correction in different hematopoietic lineages at different stages of their *in vitro* and *in vivo* differentiation. This would specify our results obtained on terminally differentiated T cells and could address one of the limitations of our study, i.e., the functional assessment of *PIK3CD* gene correction in B cells that were unfortunately counter selected by our *in vitro* activation and culture process. Finally, this approach would allow to characterize the complex interplay between multiple corrected immune cell subsets *in vivo* that will be required to mount efficient immune responses in APDS1 patients. Thus, further work is now needed to assess these aspects and gauge the feasibility and efficiency of this potentially curative approach.

For this preclinical proof of concept of *PIK3CD* gene correction, we chose to use the TALEN gene editing tool because of its maturity, specificity, and high activity. However, other gene editing tools including double-strand break-free gene editing prime editors could theoretically be used for the same endeavor. Prime editors are relatively easy to design and were shown to enable efficient gene correction at a desired locus. However, the majority of the prime editor variants described so far are not devoid of drawbacks.[36] Indeed, they can only promote the insertion of few hundred nucleotides. Insertion of larger payloads necessitate the assistance of recombinase and is still relatively inefficient for gene therapy purposes.

Nevertheless, there is no doubt that their future optimization will overcome these limitations and potentially offer an alternative technology to correct *PIK3CD*. In summary, we demonstrate that the *PIK3CD* dominant GoF mutation associated to APDS1 can be successfully corrected in APDS1 patient T cells using TALEN gene editing and AAV6-based DNA repair matrix. This correction rescues the cytolytic function of APDS1 T cells, normalizes their intracellular pAKT levels found at basal and activated states as well as the transcriptomic signature of certain genes involve in T cell cytolytic function, activation, and fitness. This successful demonstration of *PIK3CD* gene correction warrants the development of a gene therapy approach to treat p110δ dysregulations in a long-term fashion.

MATERIALS AND METHODS

Biological material

All study participants and/or their parents/guardians provided written informed consent. Research study protocols were approved by the Comité de Protection des Personnes Ile de France II, Paris, France (refs. 2015-01-05 and 2015-01-05 MS2) and the French Advisory Committee on Data Processing in Medical Research (Comité Consultatif sur le Traitement de l'Information en matière de Recherche dans le domaine de la Santé, Paris, France; ref. 15.297bis). Healthy donor PBMCs were obtained from the Etablissement Français du Sang. PBMCs were cultured in X-VIVO 15 Media (Lonza, cat. no. BE04-418Q), containing IL-2 (Miltenyi Biotech, cat. no. 130-097-748) and human serum AB (Biowest, cat. no. S4190).

B-EBV cells were immortalized from B cells originating from a HD as described previously.[37] They were cultivated in RPMI (Gibco, cat. no. 61870044) supplemented with FBS (Gibco, cat. no. 10270). B-EBV cells were transduced with luciferase-mCherry-lentivirus at a multiplicity of infection (MOI) of 10. The lentiviral plasmid encoding a firefly luciferase protein (pEFS-eFFLY-mCherry) was kindly provided by Dr. Mathias Titteux. Cells were sorted and called B-EBV-luc.

Gene editing procedure

PBMCs were activated with 20 nM phorbol myristate acetate/1 μM ionomycin for 2 days. After an additional 4 days of culture with 20 ng/mL (IL-2) 5×10^6 T cells were resuspended in cytoporation buffer T and electroporated using BTX Harvard apparatus in 0.4 cm cuvettes with 15 μg of each TALEN arm mRNA (Table S1). The electroporated cells were then immediately transferred to a 12-well plate containing 1 mL of prewarmed X-VIVO 15 serum-free media and incubated at 37°C for 15 min. The cells were then concentrated to 8E−6 cells/mL in 250 μL of the same medium in the presence of AAV6 particles (MOI = 10E−5 vg/cells) comprising the donor matrices (Table S2) in 48-well plates. After 2 h of culture at 30°C, 250 μL of X-VIVO 15 media supplemented by 10% AB serum and 40 ng/mL IL-2 was added to the cell suspension, and the mix was incubated for 24 h under the same culture conditions. One day later, the cells were seeded at a density of 10^6 cells/mL in complete X-VIVO 15 media and cultivated at 37°C in the presence of 5% CO_2. Cells were further cultured in medium containing IL-2 changed every 2 days.

Quantification of TALEN efficiency by ddPCR and next-generation sequencing

DNA was extracted 10 days after electroporation to assess the cleavage frequency of the TALEN by ddPCR. Two assays were set up to quantify both indels and HDR events. The first assay uses one probe was specific to the TALEN cut site: when indels are generated the probe does not bind and its loss can be quantified. In the second assay, codon-optimized *PIK3CD* is recognized by a specific probe. Both assays are normalized with an internal probe quantifying RPP30. Primers and probes used are described in Table S3.

Genomic DNA was recovered, sheared, end-repaired/A-tailed, processed, and analyzed by high-throughput DNA sequencing as described previously.[38] The frequency of indels were quantitatively assessed.

Flow cytometry and purification

Corrected cells expressing ΔLNGFR were stained using PE anti-ΔLNGFR antibody (Miltenyi, no. 130-113-421) and purified using an anti-PE MicroBeads kit (Miltenyi, no. 130-048-801) on mass spectrometry column. Cells before purification and cells from the positive and negative fraction were stained with fixable viability dye 450 and analyzed by flow cytometry.

Prime flow assay

Seven days after electroporation, cells were subjected to prime flow analysis following the manufacturer's instruction kit (Prime Flow assay kit, Thermo Fisher Scientific, cat. no. 8-18005-210). The probes used are indicated in Table S4. ΔLNGFR and viability staining (FVD450, eBioscience cat. no. 65-0863-13) were carried out during the procedure. Expression was analyzed on a flow cytometer.

pAKT quantification

Seven days after electroporation, cells were either left untouched (basal ∅ condition), treated with Pi3kinase δ inhibitor (Merck, cat. no. IC87114) or activated with 1 μg of OKT3 (Miltenyi, cat. no. 130-093-387). Cells were stained with fixable viability dye 450 and ΔLNGFR-PE before fixation and permeabilization with methanol. Intracellular staining was carried out with APC anti pAKT antibody (Cell Signaling, no. 11962). pAKT expression was assessed using flow cytometry.

Serial killing assay

To assess the cytotoxic activity of patient T cells, a serial killing assay was performed using a protocol similar to that described previously.[38] To allow recognition of B-EBVs by T cells, blinatumomab[39] a bispecific antibody crosslinking CD3 and CD19 was added. In brief, T cells were mixed with a suspension of 1×10^5 B-EBV-luc cells at E:T = 5:1 in a total volume of 500 μL of X-VIVO 15 media supplemented with 10% AB serum, 5 ng/mL of blinatumomab, and 20 ng/mL IL-2. The mixture was incubated for 24 h before determining the luminescence of 25 μL of cell suspension using 25 μL of ONE-Glo reagent (Promega, cat. no. E6110). The cell mixture was then spun down, and the old medium was discarded and substituted with 500 μL of fresh complete

X-VIVO 15 media containing 1×10^5 B-EBV-Luc cells and 5 ng/mL of blinatumomab and 20 ng/mL IL-2. The resulting cell mixture was incubated for 24 h. This protocol was repeated for 7 days. Flow cytometry staining to analyze mCherry, CD3 (FITC, Miltenyi Biotech, cat. no. 130-113-136) and viability (FVD450) was carried out on days 0, 3, and 7. Area under the curve values were computed using PRISM for each condition, statistical differences were calculated using a t test.

scRNA-seq

The scRNA-seq libraries were generated using the Chromium Single Cell Next GEM 3′ Library & Gel Bead Kit v.3.1 (10X Genomics) according to the manufacturer's protocol. In brief, cells were counted, diluted at 1,000 cells/μL in PBS+0.04% and 20,000 cells were loaded in the 10X Chromium Controller to generate single-cell gel beads in emulsion. After reverse transcription, gel beads in emulsion were disrupted. Barcoded complementary DNA was isolated and amplified by PCR. Following fragmentation, end repair and A-tailing, sample indexes were added during index PCR. The purified libraries were sequenced on a NovaSeq 6000 (Illumina) with 28 cycles of read 1, 8 cycles of i7 index, and 91 cycles of read 2.

Sequencing reads were demultiplexed and aligned to the human reference genome (GRCh38, release 98, built from Ensembl sources), using the CellRanger Pipeline v.3.1. Unfiltered RNA UMI counts were loaded into Seurat v.3.168 for quality control, data integration and downstream analyses. Apoptotic cells and empty sequencing capsules were excluded by filtering out T cells with fewer than 500 features or a mitochondrial content higher than 20%. Data from each sample were log-normalized and scaled, before batch correction using Seurat's FindTransferAnchors. The query was then mapped to the pbmc_multimodal.h5seurat reference dataset.[31] On this integrated dataset, principal-component analysis using the reduction model weighted nearest neighbor analysis. Cell-type labels were assigned to resulting clusters based on a manually curated list of marker genes as well as previously defined signatures of the well-known PBMC subtypes. Since APDS1 and HD donors were not sex-matched we removed all the genes from chromosomes X and Y. In total 74,373 cells across 10 samples were kept for further analysis. DEG analyses were conducted using the FindMarkers function of Seurat on the RNA assay with default parameters. Genes with an absolute value of avg_$\log_2$(FC) > 0.5 and adjusted $p < 0.05$ were selected as significant. Heatmaps were drawn using the Seurat's DoHeatmap function after calculating the average gene expression using AverageExpression. The function AddModuleScore was used to select the cells expressing the *PIK3CD*$_{8\text{-}24}$ cassette among the bulk *PIK3CD*$_{8\text{-}24}$-EF1-ΔLNGFR samples. The cells that had an expression over 1 were selected as positive. The function CellCycleScoring was used to extract CD8 proliferating in G2M phase. Gene ontology analysis was performed using ShinyGO.[40]

DATA AND CODE AVAILABILITY

All data presented in this work are available from the authors upon request.

SUPPLEMENTAL INFORMATION

Supplemental information can be found online at https://doi.org/10.1016/j.omtm.2023.101133.

ACKNOWLEDGMENTS

S.K. is a Centre National de la Recherche Scientifique staff researcher. We thank the CRB-DNA from Necker for the establishment of immortalized B-EBV; the Etablissement Français du Sang for blood supply from healthy donors; the cytometry platform from Necker; the Human Lymphohematopoiesis laboratory for discussion. The LabTech Single-Cell@Imagine, was supported by the Paris Region and the "Investissement d'avenir" program through 2019 ATF funding—Sésame Filières PIA (grant 3877871). Cellectis and Imagine would like to thank the generous contribution of all the patients involved in this study. Some schemes were created with biorender.com.

AUTHOR CONTRIBUTIONS

S.K., P.D., A.J., and M.C., designed the study. P.D. and A.J. designed the gene editing strategy including TALEN design and AAV6 repair matrix in collaboration with S.K. J.V. participated in the design of the functional readouts. L.P. performed most of the experiments and analyzed data. L.C. helped setting up cell culture conditions and functional readouts. S.L. designed and optimized the ddPCR assays. M.L. prepared and sequenced the single-cell libraries. F.C. computed the single-cell RNA sequencing data and L.P. plotted the transcriptomics data. A.M. participated in the analysis of single-cell RNA sequencing data and managed S.L. M.M. managed M.L. and F.C. for single-cell RNA sequencing dataset acquisition and computing. L.P., J.V., and S.K. analyzed data and wrote the manuscript with the input of all authors. J.V. and S.K. supervised the study.

DECLARATION OF INTERESTS

S.L., A.B., A.J., A.M., P.D., and J.V. are Cellectis employees. TALEN is a Cellectis patented technology. M.C. has consulted for Cellectis. S.K. reports collaboration agreements and payments from Cellectis. J.V., P.D., A.J., L.P., M.C., and S.K. are inventors on an EP patent application related to this work.

REFERENCES

1. Lucas, C.L., Kuehn, H.S., Zhao, F., Niemela, J.E., Deenick, E.K., Palendira, U., Avery, D.T., Moens, L., Cannons, J.L., Biancalana, M., et al. (2014). Dominant-Activating, Germline Mutations in Phosphoinositide 3-Kinase p110δ Cause T Cell Senescence and Human Immunodeficiency. Nat. Immunol. *15*, 88–97. https://doi.org/10.1038/ni.2771.

2. Angulo, I., Vadas, O., Garçon, F., Banham-Hall, E., Plagnol, V., Leahy, T.R., Baxendale, H., Coulter, T., Curtis, J., Wu, C., et al. (2013). Phosphoinositide 3-kinase δ gene mutation predisposes to respiratory infection and airway damage. Science *342*, 866–871. https://doi.org/10.1126/science.1243292.

3. Coulter, T.I., Chandra, A., Bacon, C.M., Babar, J., Curtis, J., Screaton, N., Goodlad, J.R., Farmer, G., Steele, C.L., Leahy, T.R., et al. (2017). Clinical spectrum and features of activated phosphoinositide 3-kinase δ syndrome: A large patient cohort study. J. Allergy Clin. Immunol. *139*, 597–606.e4. https://doi.org/10.1016/j.jaci.2016.06.021.

4. Vanhaesebroeck, B., Welham, M.J., Kotani, K., Stein, R., Warne, P.H., Zvelebil, M.J., Higashi, K., Volinia, S., Downward, J., and Waterfield, M.D. (1997). P110delta, a

novel phosphoinositide 3-kinase in leukocytes. Proc. Natl. Acad. Sci. USA *94*, 4330–4335. https://doi.org/10.1073/pnas.94.9.4330.

5. Heurtier, L., Lamrini, H., Chentout, L., Deau, M.-C., Bouafia, A., Rosain, J., Plaza, J.-M., Parisot, M., Dumont, B., Turpin, D., et al. (2017). Mutations in the adaptor-binding domain and associated linker region of p110δ cause Activated PI3K-δ Syndrome 1 (APDS1). Haematologica *102*, e278–e281. https://doi.org/10.3324/haematol.2017.167601.

6. Rae, W., Gao, Y., Ward, D., Mattocks, C.J., Eren, E., and Williams, A.P. (2017). A novel germline gain-of-function variant in PIK3CD. Clin. Immunol. *181*, 29–31. https://doi.org/10.1016/j.clim.2017.05.020.

7. Sogkas, G., Fedchenko, M., Dhingra, A., Jablonka, A., Schmidt, R.E., and Atschekzei, F. (2018). Primary immunodeficiency disorder caused by phosphoinositide 3-kinase δ deficiency. J. Allergy Clin. Immunol. *142*, 1650–1653.e2. https://doi.org/10.1016/j.jaci.2018.06.039.

8. Swan, D.J., Aschenbrenner, D., Lamb, C.A., Chakraborty, K., Clark, J., Pandey, S., Engelhardt, K.R., Chen, R., Cavounidis, A., Ding, Y., et al. (2019). Immunodeficiency, autoimmune thrombocytopenia and enterocolitis caused by autosomal recessive deficiency of PIK3CD-encoded phosphoinositide 3-kinase δ. Haematologica *104*, e483–e486. https://doi.org/10.3324/haematol.2018.208397.

9. Maccari, M.E., Abolhassani, H., Aghamohammadi, A., Aiuti, A., Aleinikova, O., Bangs, C., Baris, S., Barzaghi, F., Baxendale, H., Buckland, M., et al. (2018). Disease Evolution and Response to Rapamycin in Activated Phosphoinositide 3-Kinase δ Syndrome: The European Society for Immunodeficiencies-Activated Phosphoinositide 3-Kinase δ Syndrome Registry. Front. Immunol. *9*, 543. https://doi.org/10.3389/fimmu.2018.00543.

10. Rao, V.K., Webster, S., Šedivá, A., Plebani, A., Schuetz, C., Shcherbina, A., Conlon, N., Coulter, T., Dalm, V.A., Trizzino, A., et al. (2023). A randomized, placebo-controlled phase 3 trial of the PI3Kδ inhibitor leniolisib for activated PI3Kδ syndrome. Blood *141*, 971–983. https://doi.org/10.1182/blood.2022018546.

11. Rao, V.K., Webster, S., Dalm, V.A.S.H., Šedivá, A., van Hagen, P.M., Holland, S., Rosenzweig, S.D., Christ, A.D., Sloth, B., Cabanski, M., et al. (2017). Effective "activated PI3Kδ syndrome"-targeted therapy with the PI3Kδ inhibitor leniolisib. Blood *130*, 2307–2316. https://doi.org/10.1182/blood-2017-08-801191.

12. Diaz, N., Juarez, M., Cancrini, C., Heeg, M., Soler-Palacín, P., Payne, A., Johnston, G.I., Helmer, E., Cain, D., Mann, J., et al. (2020). Seletalisib for Activated PI3Kδ Syndromes: Open-Label Phase 1b and Extension Studies. J. Immunol. *205*, 2979–2987. https://doi.org/10.4049/jimmunol.2000326.

13. Dimitrova, D., Nademi, Z., Maccari, M.E., Ehl, S., Uzel, G., Tomoda, T., Okano, T., Imai, K., Carpenter, B., Ip, W., et al. (2022). International retrospective study of allogeneic hematopoietic cell transplantation for activated PI3K-delta syndrome. J. Allergy Clin. Immunol. *149*, 410–421.e7. https://doi.org/10.1016/j.jaci.2021.04.036.

14. Takeda, A.J., Zhang, Y., Dornan, G.L., Siempelkamp, B.D., Jenkins, M.L., Matthews, H.F., McElwee, J.J., Bi, W., Seeborg, F.O., Su, H.C., et al. (2017). Novel PIK3CD mutations affecting N-terminal residues of p110δ cause APDS1 in humans. J. Allergy Clin. Immunol. *140*, 1152–1156.e10. https://doi.org/10.1016/j.jaci.2017.03.026.

15. Crank, M.C., Grossman, J.K., Moir, S., Pittaluga, S., Buckner, C.M., Kardava, L., Agharahimi, A., Meuwissen, H., Stoddard, J., Niemela, J., et al. (2014). Mutations in PIK3CD Can Cause Hyper IgM Syndrome (HIGM) Associated with Increased Cancer Susceptibility. J. Clin. Immunol. *34*, 272–276. https://doi.org/10.1007/s10875-014-0012-9.

16. Dulau Florea, A.E., Braylan, R.C., Schafernak, K.T., Williams, K.W., Daub, J., Goyal, R.K., Puck, J.M., Rao, V.K., Pittaluga, S., Holland, S.M., et al. (2017). Abnormal B-Cell Maturation in the Bone Marrow of Patients with Germline Mutations in PIK3CD. J. Allergy Clin. Immunol. *139*, 1032–1035.e6. https://doi.org/10.1016/j.jaci.2016.08.028.

17. Luo, Y., Xia, Y., Wang, W., Li, Z., Jin, Y., Gong, Y., He, T., Li, Q., Li, C., and Yang, J. (2018). Identification of a novel *de novo* gain-of-function mutation of PIK3CD in a patient with activated phosphoinositide 3-kinase δ syndrome. Clin. Immunol. *197*, 60–67. https://doi.org/10.1016/j.clim.2018.08.007.

18. Thauland, T.J., Pellerin, L., Ohgami, R.S., Bacchetta, R., and Butte, M.J. (2019). Case Study: Mechanism for Increased Follicular Helper T Cell Development in Activated PI3K Delta Syndrome. Front. Immunol. *10*, 753. https://doi.org/10.3389/fimmu.2019.00753.

19. Tessarin, G., Rossi, S., Baronio, M., Gazzurelli, L., Colpani, M., Benvenuto, A., Zunica, F., Cardinale, F., Martire, B., Brescia, L., et al. (2020). Activated Phosphoinositide 3-Kinase Delta Syndrome 1: Clinical and Immunological Data from an Italian Cohort of Patients. J. Clin. Med. *9*, 3335. https://doi.org/10.3390/jcm9103335.

20. Wentink, M., Dalm, V., Lankester, A.C., van Schouwenburg, P.A., Schölvinck, L., Kalina, T., Zachova, R., Sediva, A., Lambeck, A., Pico-Knijnenburg, I., et al. (2017). Genetic defects in PI3Kδ affect B-cell differentiation and maturation leading to hypogammaglobulineamia and recurrent infections. Clin. Immunol. *176*, 77–86. https://doi.org/10.1016/j.clim.2017.01.004.

21. Rodriguez, R., Fournier, B., Cordeiro, D.J., Winter, S., Izawa, K., Martin, E., Boutboul, D., Lenoir, C., Fraitag, S., Kracker, S., et al. (2019). Concomitant PIK3CD and TNFRSF9 deficiencies cause chronic active Epstein-Barr virus infection of T cells. J. Exp. Med. *216*, 2800–2818. https://doi.org/10.1084/jem.20190678.

22. Ren, J., Liu, X., Fang, C., Jiang, S., June, C.H., and Zhao, Y. (2017). Multiplex Genome Editing to Generate Universal CAR T Cells Resistant to PD1 Inhibition. Clin. Cancer Res. *23*, 2255–2266. https://doi.org/10.1158/1078-0432.CCR-16-1300.

23. Hubbard, N., Hagin, D., Sommer, K., Song, Y., Khan, I., Clough, C., Ochs, H.D., Rawlings, D.J., Scharenberg, A.M., and Torgerson, T.R. (2016). Targeted gene editing restores regulated CD40L function in X-linked hyper-IgM syndrome. Blood *127*, 2513–2522. https://doi.org/10.1182/blood-2015-11-683235.

24. Bonini, C., Grez, M., Traversari, C., Ciceri, F., Marktel, S., Ferrari, G., Dinauer, M., Sadat, M., Aiuti, A., Deola, S., et al. (2003). Safety of retroviral gene marking with a truncated NGF receptor. Nat. Med. *9*, 367–369. https://doi.org/10.1038/nm0403-367.

25. Dolmetsch, R.E., Lewis, R.S., Goodnow, C.C., and Healy, J.I. (1997). Differential activation of transcription factors induced by Ca2+ response amplitude and duration. Nature *386*, 855–858. https://doi.org/10.1038/386855a0.

26. Dadsetan, S., Shishkin, V., and Fomina, A.F. (2005). Intracellular Ca(2+) release triggers translocation of membrane marker FM1-43 from the extracellular leaflet of plasma membrane into endoplasmic reticulum in T lymphocytes. J. Biol. Chem. *280*, 16377–16382. https://doi.org/10.1074/jbc.M501202200.

27. Frey, M.R., Leontieva, O., Watters, D.J., and Black, J.D. (2001). Stimulation of protein kinase C-dependent and -independent signaling pathways by bistratene A in intestinal epithelial cells. Biochem. Pharmacol. *61*, 1093–1100. https://doi.org/10.1016/s0006-2952(01)00596-2.

28. Asano, T., Okada, S., Tsumura, M., Yeh, T.-W., Mitsui-Sekinaka, K., Tsujita, Y., Ichinose, Y., Shimada, A., Hashimoto, K., Wada, T., et al. (2018). Enhanced AKT Phosphorylation of Circulating B Cells in Patients With Activated PI3Kδ Syndrome. Front. Immunol. *9*, 568. https://doi.org/10.3389/fimmu.2018.00568.

29. Wang, Y., Wang, W., Liu, L., Hou, J., Ying, W., Hui, X., Zhou, Q., Liu, D., Yao, H., Sun, J., and Wang, X. (2018). Report of a Chinese Cohort with Activated Phosphoinositide 3-Kinase δ Syndrome. J. Clin. Immunol. *38*, 854–863. https://doi.org/10.1007/s10875-018-0568-x.

30. Zhu, M., Wu, B., Brandl, C., Johnson, J., Wolf, A., Chow, A., and Doshi, S. (2016). Blinatumomab, a Bispecific T-cell Engager (BiTE(®)) for CD-19 Targeted Cancer Immunotherapy: Clinical Pharmacology and Its Implications. Clin. Pharmacokinet. *55*, 1271–1288. https://doi.org/10.1007/s40262-016-0405-4.

31. Hao, Y., Hao, S., Andersen-Nissen, E., Mauck, W.M., Zheng, S., Butler, A., Lee, M.J., Wilk, A.J., Darby, C., Zager, M., et al. (2021). Integrated analysis of multimodal single-cell data. Cell *184*, 3573–3587.e29. https://doi.org/10.1016/j.cell.2021.04.048.

32. Lindeboom, R.G.H., Vermeulen, M., Lehner, B., and Supek, F. (2019). The impact of nonsense-mediated mRNA decay on genetic disease, gene editing and cancer immunotherapy. Nat. Genet. *51*, 1645–1651. https://doi.org/10.1038/s41588-019-0517-5.

33. Colella, P., Ronzitti, G., and Mingozzi, F. (2018). Emerging Issues in AAV-Mediated In Vivo Gene Therapy. Mol. Ther. Methods Clin. Dev. *8*, 87–104. https://doi.org/10.1016/j.omtm.2017.11.007.

34. Fang, Y., Xue, J.-L., Shen, Q., Chen, J., and Tian, L. (2012). MicroRNA-7 inhibits tumor growth and metastasis by targeting the phosphoinositide 3-kinase/Akt pathway in hepatocellular carcinoma. Hepatology *55*, 1852–1862. https://doi.org/10.1002/hep.25576.

35. Wang, X., Chang, W.-C., Wong, C.W., Colcher, D., Sherman, M., Ostberg, J.R., Forman, S.J., Riddell, S.R., and Jensen, M.C. (2011). A transgene-encoded cell surface polypeptide for selection, *in vivo* tracking, and ablation of engineered cells. Blood *118*, 1255–1263. https://doi.org/10.1182/blood-2011-02-337360.

36. Chen, P.J., and Liu, D.R. (2023). Prime editing for precise and highly versatile genome manipulation. Nat. Rev. Genet. *24*, 161–177. https://doi.org/10.1038/s41576-022-00541-1.

37. Tosato, G., and Cohen, J.I. (2007). Generation of Epstein-Barr Virus (EBV)–Immortalized B Cell Lines. Curr. Protoc. Im. *76*, 7.22.1–7.22.4. https://doi.org/10.1002/0471142735.im0722s76.

38. Sachdeva, M., Busser, B.W., Temburni, S., Jahangiri, B., Gautron, A.-S., Maréchal, A., Juillerat, A., Williams, A., Depil, S., Duchateau, P., et al. (2019). Repurposing endogenous immune pathways to tailor and control chimeric antigen receptor T cell functionality. Nat. Commun. *10*, 5100. https://doi.org/10.1038/s41467-019-13088-3.

39. Löffler, A., Kufer, P., Lutterbüse, R., Zettl, F., Daniel, P.T., Schwenkenbecher, J.M., Riethmüller, G., Dörken, B., and Bargou, R.C. (2000). A recombinant bispecific single-chain antibody, CD19 x CD3, induces rapid and high lymphoma-directed cytotoxicity by unstimulated T lymphocytes. Blood *95*, 2098–2103.

40. Ge, S.X., Jung, D., and Yao, R. (2020). ShinyGO: a graphical gene-set enrichment tool for animals and plants. Bioinformatics *36*, 2628–2629. https://doi.org/10.1093/bioinformatics/btz931.